CHEMISTRY
A European Journal

A Journal of
ChemPubSoc Europe

Accepted Article

Title: Mechanism and Origin of Stereoselectivity in Chiral Phosphoric Acid-Catalysed Aldol-Type Reactions of Azlactones with Vinyl Ethers

Authors: Kyohei Kanomata, Yuki Nagasawa, Masahiro Yamanaka, Yukihiro Shibata, Fuyuki Egawa, Jun Kikuchi, and Masahiro Terada

To be cited as: *Chem. Eur. J.* 10.1002/chem.201905296

Link to VoR: http://dx.doi.org/10.1002/chem.201905296

Supported by
ACES

WILEY-VCH

10.1002/chem.201905296

WILEY-VCH

FULL PAPER

Mechanism and Origin of Stereoselectivity in Chiral Phosphoric Acid-Catalysed Aldol-Type Reactions of Azlactones with Vinyl Ethers

Kyohei Kanomata,[a],[‡] Yuki Nagasawa,[b] Yukihiro Shibata,[b] Masahiro Yamanaka,*[b] Fuyuki Egawa,[a] Jun Kikuchi,[a] and Masahiro Terada*[a]

Abstract: The precise mechanism of the chiral phosphoric acid-catalysed aldol-type reaction of azlactones with vinyl ethers was investigated. DFT calculations suggested that the reaction proceeds through a Conia-ene-type transition state consisting of the vinyl ether and the enol tautomer of the azlactone, in which the catalyst protonates the nitrogen atom of the azlactone to promote enol tautomerization. In addition, the phosphoryl oxygen of the catalyst interacts with the vinyl proton of the vinyl ether. The favorable transition structure features dicoordinating hydrogen bonds. However, these hydrogen bonds are not involved in the bond recombination sequence and hence the catalyst functions as a template for binding substrates. From the results of theoretical studies and experimental supports, the high enantioselectivity is induced by the steric repulsion between the azlactone substituent and the binaphthyl backbone of the catalyst under the catalyst template effect.

Introduction

The development of enantioselective catalysis using a chiral Brønsted acid has evolved into an active research field over the past few decades.[1] In particular, BINOL (1,1'-bi-2-naphthol)-derived chiral phosphoric acids **1**, shown in Scheme 1, have emerged as privileged organocatalysts[2,3] and a broad range of enantioselective reactions have been established using **1** and its derivatives. The wide applicability of those acid catalysts has stimulated mechanistic elucidation not only of stereochemical control but also of the reaction pathway, and tremendous efforts have been devoted to identify the chiral Brønsted acid catalysis. Among the approaches endeavored, DFT calculations have proven to be a powerful tool for elucidating the mechanisms of a range of reactions catalysed by **1** and its derivatives.[4-6]

[a] Dr. K. Kanomata, F. Egawa, Dr. J. Kikuchi, Prof. Dr. M. Terada
Department of Chemistry, Graduate School of Science, Tohoku University
Aramaki, Aoba-ku, Sendai 980-8578 (Japan)
E-mail: mterada@m.tohoku.ac.jp
[b] Y. Nagasawa, Y. Shibata, Prof. Dr. M. Yamanaka
Department of Chemistry and Research Center for Smart Molecules, Faculty of Science, Rikkyo University
3-34-1 Nishi-Ikebukuro, Toshima-ku, Tokyo 171-8501, Japan
E-mail: myamanak@rikkyo.ac.jp
[‡] Present Addresses: Department of Agro-Environmental Sciences, Graduate School of Bioresource and Bioenvironmental Sciences, Kyushu University, Fukuoka 819-0395, Japan

Supporting information for this article is given via a link at the end of the document.

We previously developed the chiral phosphoric acid-catalysed enantioselective aldol-type reaction of vinyl ethers with azlactones as nucleophiles (Scheme 1).[7a] When followed by the ring opening of the azlactone unit, this reaction provides access to biologically and pharmaceutically intriguing β-hydroxy-α-amino acid derivatives in enantioenriched forms.[7,8] However, the precise reaction mechanism and the origin of the high enantio- and diastereoselectivity have remained unclear. In addition, the stereoselectivity is intriguingly dependent on substituent Ar at the 2-position of the azlactone,[7a,9] even though the substituent is introduced at the far side from the reaction site that is the 4-position of the azlactone.

Two reaction mechanisms have been proposed for the present aldol-type reaction.[7a,10] We originally proposed a stepwise reaction mechanism in which the vinyl ether is protonated by the catalyst to form oxocarbenium intermediate **I**, followed by the stereoselective nucleophilic addition of the azlactone (Scheme 1).[7a] On the other hand, Tepe and Fisk proposed Conia-ene-type six-membered cyclic transition state **II** for the thermal reaction, namely, without using a catalyst, based on the fact that the stereospecific *syn*-addition of the azlactone to the vinyl ether was observed experimentally (Scheme 2).[10] DFT studies are a promising approach for clarifying the mechanism of the present aldol-type reaction. Herein we report detailed DFT studies of this reaction and disclose that the reaction proceeds *via* a six-membered Conia-ene-type cyclic transition state and not through the stepwise mechanism proposed previously.[7a] Of

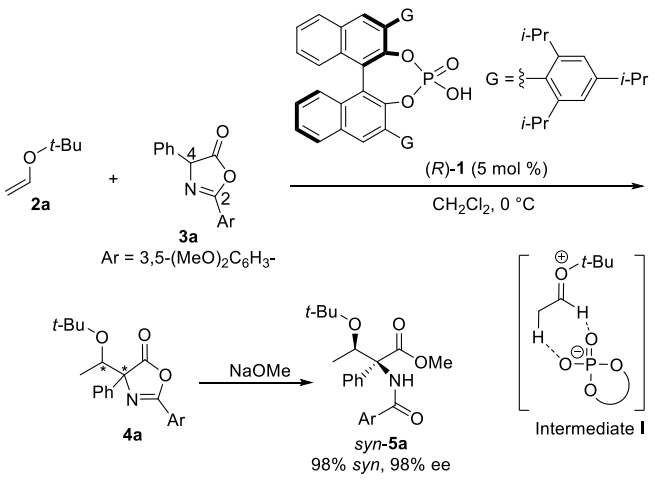

Scheme 1. Our previous work: Enantioselective reaction of vinyl ether with azlactone catalysed by chiral phosphoric acid (*R*)-**1**.

10.1002/chem.201905296

Scheme 2 Reported by Tepe and Fisk: Stereospecific reaction of vinyl ethers with azlactones without a catalyst.

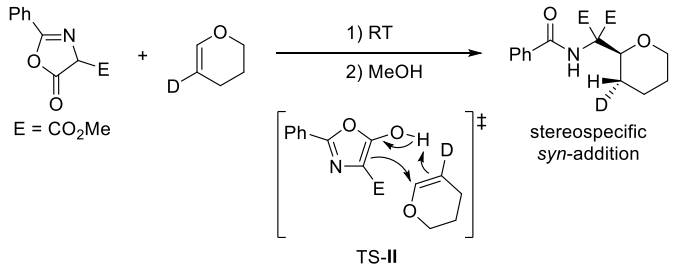

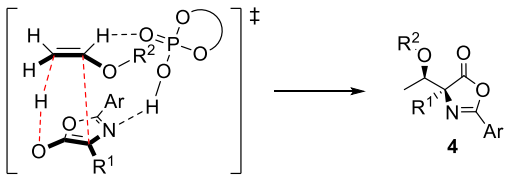

Figure 1. Theoretically elucidated Conia-ene-type cyclic transition state of chiral phosphoric acid-catalysed reaction.

particular interest is that chiral phosphoric acid catalyst is not involved in the bond recombination sequence of the Conia-ene-type cyclic transition state and the catalyst functions as a template for binding both substrates, the vinyl ether and the azlactone, through hydrogen bonds (Figure 1). In addition, the intriguing substituent effect of Ar introduced at the 2-position of the azlactone is well rationalized by a theoretically proposed model, in which the steric bulkiness of the Ar substituent plays a vital role in determining the stereochemical outcome. The proposed model for stereocontrol was also confirmed by further experimental support.

Results and Discussion

Chemical Models and Computational Methods

At the outset of the present study, the reaction mechanism was investigated using a simplified chemical model in order to reduce computational costs (Figure 2a). Thus, a biphenol-derived phosphoric acid (**cat**) instead of a binaphthol-derived phosphoric acid, vinyl methyl ether (**VE**), and a dimethyl-substituted azlactone (**AZ**) were used. Investigations of the steric interactions and the origin of the stereochemical outcome were then pursued employing a realistic chemical model (Figure2b) based on the located transition structures identified using the simplified chemical model. All of the calculations were performed with the Gaussian 09 package.[11] The geometries were fully optimized at the B3LYP/6-31G* level[12] and characterized using frequency calculations, and the free energies were computed for the gas phase and the solution phase according to the SCRF method based on CPCM (CH_2Cl_2). For the realistic chemical model,

(a) Simplified chemical model

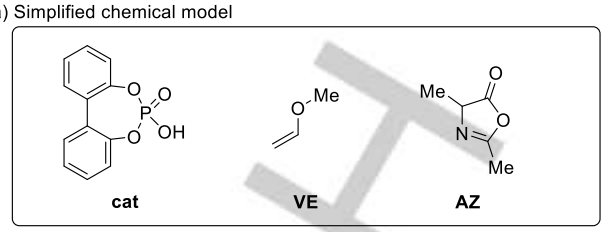

(b) Realistic chemical model

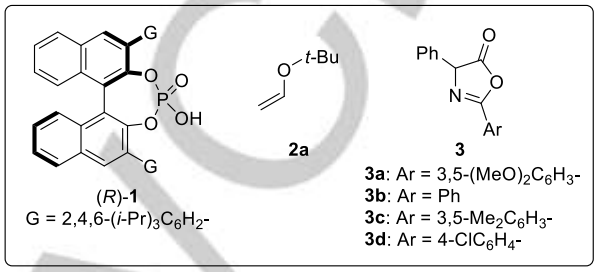

Figure 2. Chemical models for computational studies.

single-point energy calculations for the optimized structures (at the B3LYP/6-31G* level) were evaluated at the M06-2X/6-31G* level in the gas phase.[13]

Investigation of Reaction Pathway Using Simplified Chemical Model

First, reaction pathways for the present aldol-type reaction were investigated using the simplified chemical model. After intensive screening for possible transient configurations, three reaction pathways were identified in the gas phase and the solution phase according to the SCRF method based on CPCM (CH_2Cl_2) (Figure 3): a pathway involving an oxocarbenium intermediate (Path A) and pathways proceeding *via* cyclic transition structures (Paths B and C).

Path A, which is identical to the reaction mechanism originally proposed by our group,[7a] involves an oxocarbenium ion as the key reaction intermediate (Figure 3a). The reaction pathway was assumed to consist of two steps: (1) protonation of **VE** by **cat** to form an ion-paired complex between the oxocarbenium intermediate and the chiral phosphate, followed by (2) nucleophilic addition of the enol tautomer of **AZ** to the ion-paired complex. After screening for the possible structural conformations for the latter step, **TS-A** was identified as the transition state (TS) with the lowest relative energy (gas phase: ΔE = 21.7 kcal/mol, solution phase: ΔE = 16.9 kcal/mol).[14]

Other possible reaction pathways, namely, cyclic TSs, were also investigated. The transition structure along Path B (**TS-B**) features a ten-membered cyclic structure consisting of **VE**, **AZ**, and **cat** (Figure 3b). In **TS-B**, **cat** is embedded into the bond recombination sequence of the reaction. Accordingly, **cat** protonates the double bond of **VE** and captures another proton from the enol moiety of **AZ**, promoting carbon-carbon bond formation between **VE** and **AZ**. Although the transition structure of Path B has not been located in the solution phase,[15] in the gas

10.1002/chem.201905296

phase, the relative energy of **TS-B** (Δ*E* = 10.3 kcal/mol) is far lower than that of **TS-A** (Δ*E* = 21.7 kcal/mol), and thus the stepwise pathway *via* the generation of ionic intermediate **I** (see Scheme 1) is unfavorable in the present reaction.

Reactions *via* a six-membered cyclic TS (Path C) were also investigated (Figure 3c). It is noteworthy that the six-membered ring in **TS-C** consists of **VE** and **AZ**, and thus **cat** is not involved in the bond recombination sequence. Instead, **cat** protonates the nitrogen atom of **AZ**, which is the most basic site among the substrates. The protonation of **AZ** likely promotes tautomerization to the enol form and enhances the acidity of the enol proton, facilitating proton transfer from **AZ** to **VE**. A frequency calculation revealed that **TS-C** corresponds to the proton transfer step from **AZ** to **VE**. In addition, an intrinsic reaction coordinate (IRC) calculation suggested that carbon-carbon bond formation proceeds smoothly without any activation barrier soon after proton transfer. Transition structures with changing conformations in Path C ranged in relative energy from 3.5 to 10 kcal/mol,[14] and

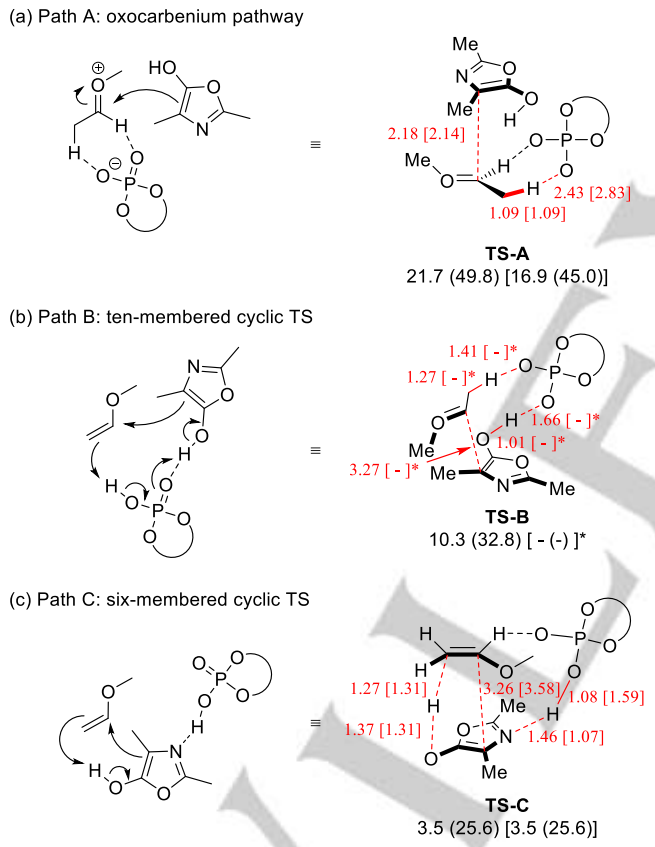

Figure 3. Transition structures located using the simplified chemical model. Relative energies of the transition state in the gas phase are shown in kcal/mol with respect to the sum of **VE**, **AZ**, and **cat**. Relative Gibbs free energies are shown in parentheses. Bond lengths of the transition structures in the gas phase are indicated in red (angstroms). Relative energies (kcal/mol) of the transition state in the solution phase were calculated at the same level according to the SCRF method based on CPCM (CH_2Cl_2) and are shown in brackets. Similarly, relative Gibbs free energies are shown in parentheses. Bond lengths in the solution phase are shown in brackets (angstroms) *In the solution phase, **TS-B** has not been located, albeit thorough screening.

TS-C was determined to be the most energetically favorable transition state (gas phase: Δ*E* = 3.5 kcal/mol, solution phase: Δ*E* = 3.5 kcal/mol). In located transition structure **TS-C**, the phosphoric acid (P-OH) of **cat** protonates the nitrogen atom of **AZ**, whereas the phosphoryl oxygen (P=O) of **cat** interacts with the vinyl proton of **VE**. Thus, **TS-C** features dicoordinating hydrogen bonds, which are an essential interaction mode observed widely in chiral phosphoric acid-catalysed reactions and are beneficial for controlling the stereochemical outcome (Figure 3c).[4-6] However, it should be emphasized that in the present transition state, these hydrogen bonds are not involved in the bond recombination sequence and **cat** functions as a template for binding both substrates, **AZ** and **VE**, of which relative locations are fixed. This finding is in stark contrast to the current understanding of the reaction mechanism under chiral phosphoric acid catalysis, and thus the dicoordinating hydrogen bonds effectively participate in the bond recombination sequence and accelerate the reaction efficiently.[4-6] As discussed above, these simplified model studies strongly suggest that Path C is the most favorable of the pathways investigated,[16] presumably because **AZ** and **VE** are well-overlapped in the transient structure of Path C[17] and hence considerable charge-separation would be avoided as compared with the other transient structures of Paths A and B.

Rationalization of Inconsistency between Previous Proposal and Theoretical Studies

As mentioned in the previous section, the theoretical study of the simplified chemical model is not consistent with our previous proposal of a stepwise mechanism as likely shown in Path A (Figure 3a).[7a] We previously proposed the mechanism on the basis of experimental evidence, as shown in Scheme 3. The reaction of (*E*)- and (*Z*)-isomers of vinyl ether **2b** with azlactone **3a** was conducted individually, followed by ring opening of the azlactone unit, to afford product **6** with exactly the same diastereo- and enantioselectivities, irrespective of the geometry of **2b**. We hence presumed that the common oxocarbenium intermediate would be generated from (*E*)- and (*Z*)-**2b** through the double bond protonation.

The experimental evidence shown in Scheme 3 is alternatively rationalized by the geometrical isomerization of vinyl ether **2b** during the course of the aldol-type reaction. We therefore monitored the isomerization of **2b** by NMR experiment. At the outset of the monitoring studies, the geometrical isomerization of **2b** on its own was monitored by ^{1}H NMR measurement under the influence of (*R*)-**1** in CD_2Cl_2 at 20 °C. As shown in Figure 4 (solid lines), both (*E*)- and (*Z*)-**2b** were isomerized under the influence of (*R*)-**1**. After 9 hours, the (*E*)/(*Z*) ratio converged into 42:58, irrespective of the starting geometry of **2b**. This clearly suggests that (*R*)-**1** facilitates the geometrical isomerization of **2b** reversibly and the isomerization reaches equilibrium after 9 hours. Similarly, in the aldol-type reaction of **2b** with **3a**, the geometrical isomerization of vinyl ether **2b** (2 equivalents of **2b** to **3a**) was observed, as shown in Figure 4 (dashed lines).[18] It should be pointed out that after 9 hours, product **6** was formed in around 70% yield in the reaction using either (*E*)- or (*Z*)-**2b**[18] and hence the reaction was not complete. Accordingly, rate of the

10.1002/chem.201905296

Scheme 3. Reaction of (*E*)- and (*Z*)-isomers of vinyl ether **2b** with azlactone **3a** catalysed by chiral phosphoric acid (*R*)-**1**.

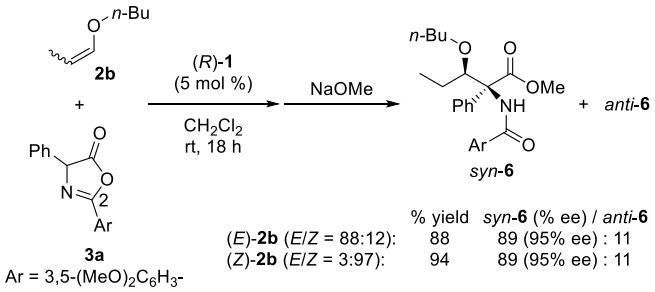

	% yield	*syn*-**6** (% ee) / *anti*-**6**
(*E*)-**2b** (*E*/*Z* = 88:12):	88	89 (95% ee) : 11
(*Z*)-**2b** (*E*/*Z* = 3:97):	94	89 (95% ee) : 11

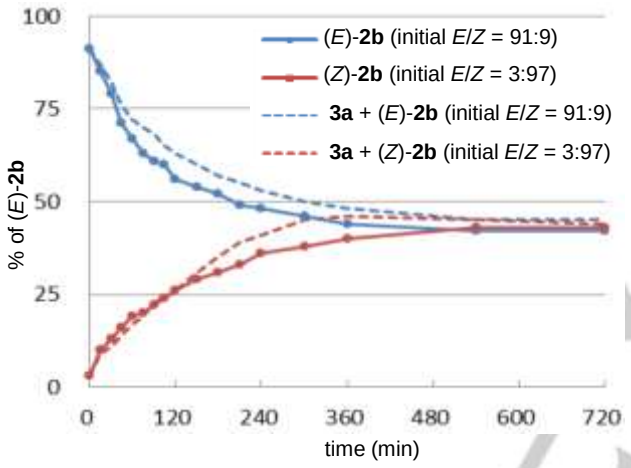

Figure 4. ^{1}H NMR monitoring of (*E*)/(*Z*) ratio of **2b** [% of (*E*)-isomer]. Solid lines: isomerization of (*E*)- or (*Z*)-**2b** (0.2 mmol) in the presence of (*R*)-**1** (0.01 mmol) in CD_2Cl_2 (0.5 mL). Dashed lines: the aldol-type reaction of (*E*)- or (*Z*)-**2b** (0.2 mmol: 2 equiv.) with **3a** (0.1 mmol) in the presence of (*R*)-**1** (0.01 mmol) in CD_2Cl_2 (0.5 mL).

geometrical isomerization is higher than that of the aldol-type reaction. More interestingly, during the course of the aldol-type reaction, the (*E*)-isomer ratio (dashed lines) is higher than that (solid lines) observed in the simple isomerization of **2b** in both cases using (*E*)- and (*Z*)-**2b**. This observation clearly indicates that (*Z*)-**2b** is consumed faster than (*E*)-**2b** in the aldol-type reaction. Consequently, it is considered that (*Z*)-**2b** is primarily involved in the aldol-type reaction even when (*E*)-**2b** is used as the initial geometrical isomer. On the basis of the rapid geometrical isomerization, coupled with the efficient resolution of the generated geometrical isomers, it could be well rationalized that exactly the same stereoselectivities were observed in the reaction using either the (*E*)- or (*Z*)-isomer of **2b**.

Clarification of Origin of Stereoselectivity Using Realistic Chemical Model

Having identified the most favorable pathway for the present aldol-type reaction, the origin of stereocontrol was further explored using the realistic chemical model based on **TS-C**. As shown in Scheme 1,[7a] the reaction of **2a** with **3a** (Ar = 3,5-$(MeO)_2C_6H_3$-) at room temperature followed by the ring opening of the azlactone unit using sodium methoxide afforded *syn*-**5a** as the major diastereomer (*syn*:*anti* = 95:5) with high enantiomeric excess (95% ee for *syn*-**5a** at room temperature), preferring (2*S*,3*R*)-**5a** over (2*R*,3*S*)-**5a**.[19] Transition structures leading to a pair of enantiomers of the *syn*-isomer (i.e., **TS-sr** and **TS-rs**) were thoroughly investigated to clarify the origins of the stereochemical outcome.[20] The experimentally observed enantioselectivities were qualitatively consistent with the calculated energy differences. The relative energy difference between **TSa-sr** and **TSa-rs** is sufficient for a high level of enantioselectivity in favor of **TSa-sr** (3.5 kcal/mol), where **TSa-sr** and **TSa-rs** correspond to the major and minor enantiomers of *syn*-**5a**, respectively (Ar = 3,5-$(MeO)_2C_6H_3$-) (Figure 5).[21]

Detailed analysis of these transition structures revealed that the observed stereocontrol can be rationalized by the following repulsive (in minor **TSa-rs**) and attractive (in major **TSa-sr**) interactions (Figures 5 and 6a). Firstly, as highlighted in the red dashed squares in Figure 5, the sterically bulky *t*-Bu group of **2a** occupies the empty pocket of catalyst **1** in energetically favored transition state **TSa-sr** (Figure 5a), whereas the *t*-Bu group engenders a steric repulsion with the 2,4,6-triisopropylphenyl group of the catalyst in disfavored transition state **TSa-rs** (Figure 5b). In contrast to the repulsive interaction, the attractive interaction stabilizes the transition structures efficiently (Figure 6a: also see Figure 7 for schematic model). In fact, energetically favorable **TSa-sr** features hydrogen bonds between the phosphoryl oxygen of **1** with the hydrogen atoms of the inside vinylic position and the *t*-Bu group in **2a** (Figure 6a: left),[22] whereas the phosphoryl oxygen in **TSa-rs** does not form any hydrogen bonds with vinyl ether **2a** (Figure 6a: right).[22] As discussed in the model studies, in energetically favorable **TSa-sr**, phosphoric acid catalyst **1** functions as a template for binding not only azlactone **3a** but also **2a** through hydrogen bonding interaction, although these hydrogen bonds are not involved in the bond recombination sequence.

As mentioned in the previous section, the NMR monitoring studies suggest that (*Z*)-**2b** is primarily involved in the aldol-type reaction, although (*E*)- and (*Z*)-geometrical mixtures are formed under the influence of the catalyst because of frequent isomerization. It is considered that the geometrical isomer of **2b** undergoes efficient resolution under energetically favorable **TSa-sr**. As highlighted by the blue dashed circle in Figure 5a, the introduction of the substituent to the vinyl ether at the (*E*)-position would lead to marked steric congestion between the vinyl substituent and the 2,4,6-triisopropylphenyl substituent of the catalyst. In contrast, the (*Z*)-position of the vinyl ether is less sterically congested and the substituent at the (*Z*)-position would not cause any steric repulsions. Consequently, the selective consumption of (*Z*)-vinyl ether in the aldol-type reaction well suits energetically favorable **TSa-sr**.

10.1002/chem.201905296

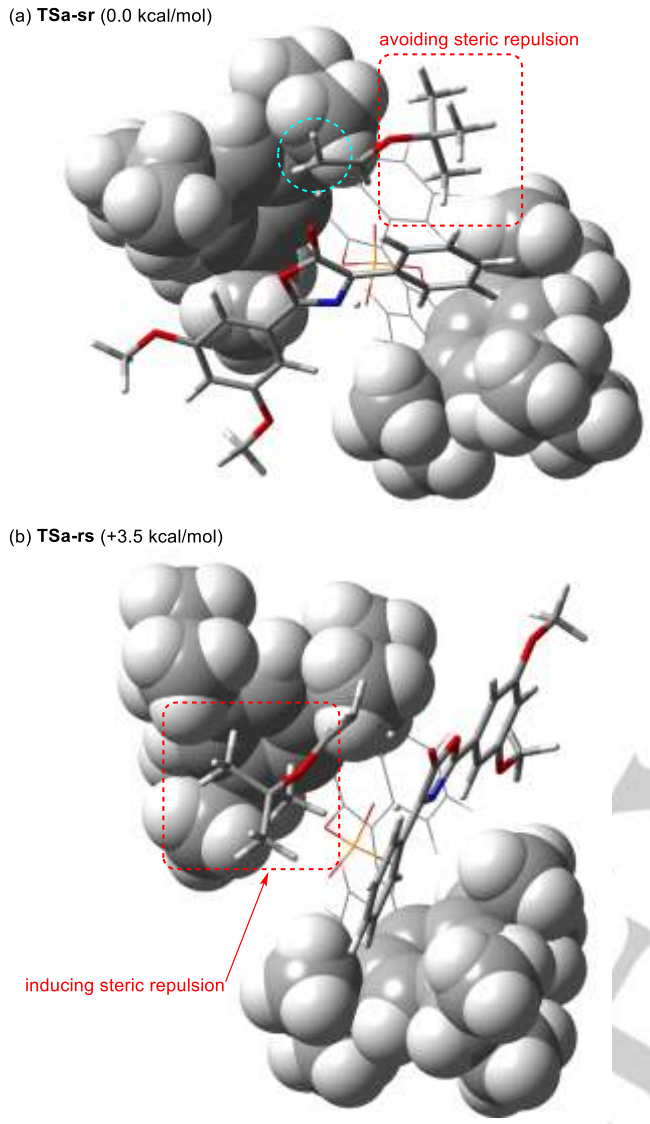

Figure 5. 3D structures of **TSa-sr** and **TSa-rs**. Relative energies of the transition state in the gas phase are shown in kcal/mol. The *t*-Bu group of **2a** is highlighted in the red dashed squares. CPK model = 2,4,6-(*i*-Pr)$_3$C$_6$H$_2$ group of catalyst (*R*)-**1**; wire model = binaphthyl backbone of (*R*)-**1**; tube model = substrates **2a** and **3**

Substituent Effect of Aryl Group at 2-Position of Azlactone

In our previous studies, the stereochemical outcome of the aldol-type reaction was found to depend markedly on the substituent (Ar) at the 2-position of azlactone **3**. In fact, the reaction of **3b** (Ar = Ph) with **2a** followed by the ring opening of the azlactone unit afforded **5b** (Ar = Ph) with moderate stereoselectivity (*syn*:*anti* = 79:21, 59% ee for *syn*-**5b** at room temperature: see section "Experimental Support" and Table 1 for a detailed discussion of the experimental results), whereas the reaction of **3a** (Ar = 3,5-(MeO)$_2$C$_6$H$_3$-)[7a] afforded corresponding **5a** with high stereoselectivity (*syn*:*anti* = 95:5, 95% ee for *syn*-**5a** at room temperature). In order to clarify the substituent effect on the enantioselectivity, we further conducted theoretical studies on the realistic chemical model of **2a** with **3b**. As shown in Figure 6b,[22] the relative energy difference between **TSb-sr** and **TSb-rs**, which are the transition structures that afford each enantiomer of *syn*-**5b** (Ar = Ph), decreased to 1.9 kcal/mol. The relative relationships of the experimentally observed enantioselectivities of *syn*-**5a** (95% ee) and *syn*-**5b** (59% ee) are qualitatively consistent with the calculated energy differences of these transition states (**TSa**s: 3.5 kcal/mol, **TSb**s: 1.9 kcal/mol).

As shown in Figure 6, the template effect of the catalyst through hydrogen bonds also stabilizes **TSb-sr** as the favorable transition state, as has been similarly observed in **TSa-sr**. Therefore, the strong dependence of the enantioselectivities on the substituents of azlactone can be rationalized by steric effects. In the reaction of azlactone **3a**, **TSa-rs**, which leads to the minor enantiomer, is destabilized by the steric repulsion between the binaphthyl backbone of the catalyst and the sterically bulky 3,5-dimethoxyphenyl group of **3a**, whereas in energetically favored **TSa-sr**, the 3,5-dimethoxyphenyl group avoids this steric congestion (Figure 6a). On the other hand, the steric effect of the corresponding phenyl group in **TSb-rs** is reduced due to the lack of methoxy groups at the 3,5-positions (Figure 6b). In fact, the H···N distance of the O···H···N hydrogen bond formed between the phosphoric acid and the azlactone is shorter in **TSb-rs** than in **TSa-rs** (1.67 Å vs. 1.70 Å) due to the decreased steric congestion in **TSb-rs**. Therefore, the energy difference between **TSb-sr** and **TSb-rs** is reduced because of the stabilization of **TSb-rs**. These results suggest that the steric bulkiness of the azlactone substituent (Ar) plays a crucial role in determining the stereochemical outcome.

Next, in order to acquire detailed insights into the origin of the energy differences between the transition states, a distortion/interaction analysis of **TSa**s was conducted (Figure 7).[23] Each transition structure was divided into catalyst and substrates moieties as separate fragments, and the degree of distortion (ΔE_{dist}) was estimated by comparing the energies of each fragment determined using single-point energy calculations at the M06-2X/6-31G* level. The interaction energies between the catalyst and the substrates (E_{int}) were also compared, and E_{int} was calculated as follows:

$$E_{int} = E_{TS} - (E_{cat} + E_{sub}),$$

where E_{TS}, E_{cat}, and E_{sub} represent the energies of the transition state, the catalyst, and combined substrates **2a** and **3**, respectively. Analysis of the highly enantioselective reaction of **3a** revealed that the interaction energy difference is dominant (ΔE_{int} = +5.6 kcal/mol) in inducing the relative energy difference between **TSa-sr** and **TSa-rs**, whereas the distortion energies are less significant (ΔE_{dist} = -0.8 and -1.3 kcal/mol). These results strongly suggest that favorable interactions are realized due to the formation of hydrogen bonds and the minimization of steric repulsions in **TSa-sr**. On the other hand, analysis of the reaction of **3b** indicated that the interaction energy difference (ΔE_{int}) is decreased to +4.0 kcal/mol (Figure S6b), which is reflected in the lower enantioselectivity, whereas the distortion energies (ΔE_{dist} = -0.8 and -1.3 kcal/mol) remain unchanged compared to those for the reaction of **3a**. It is confirmed again that the steric bulkiness

10.1002/chem.201905296

(a) **TSa-sr** and **TSa-rs** : Ar = 3,5-$(MeO)_2C_6H_3$ (95% ee)

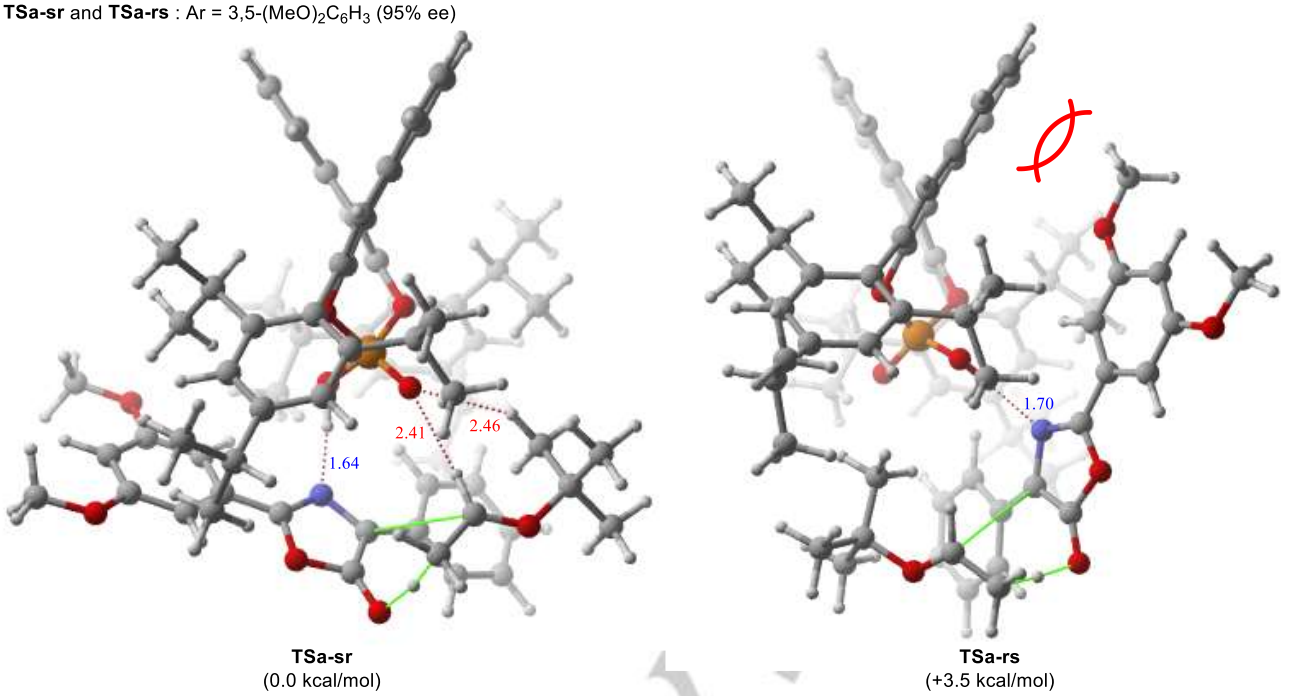

TSa-sr
(0.0 kcal/mol)

TSa-rs
(+3.5 kcal/mol)

(b) **TSb-sr** and **TSb-rs** : Ar = Ph (59% ee)

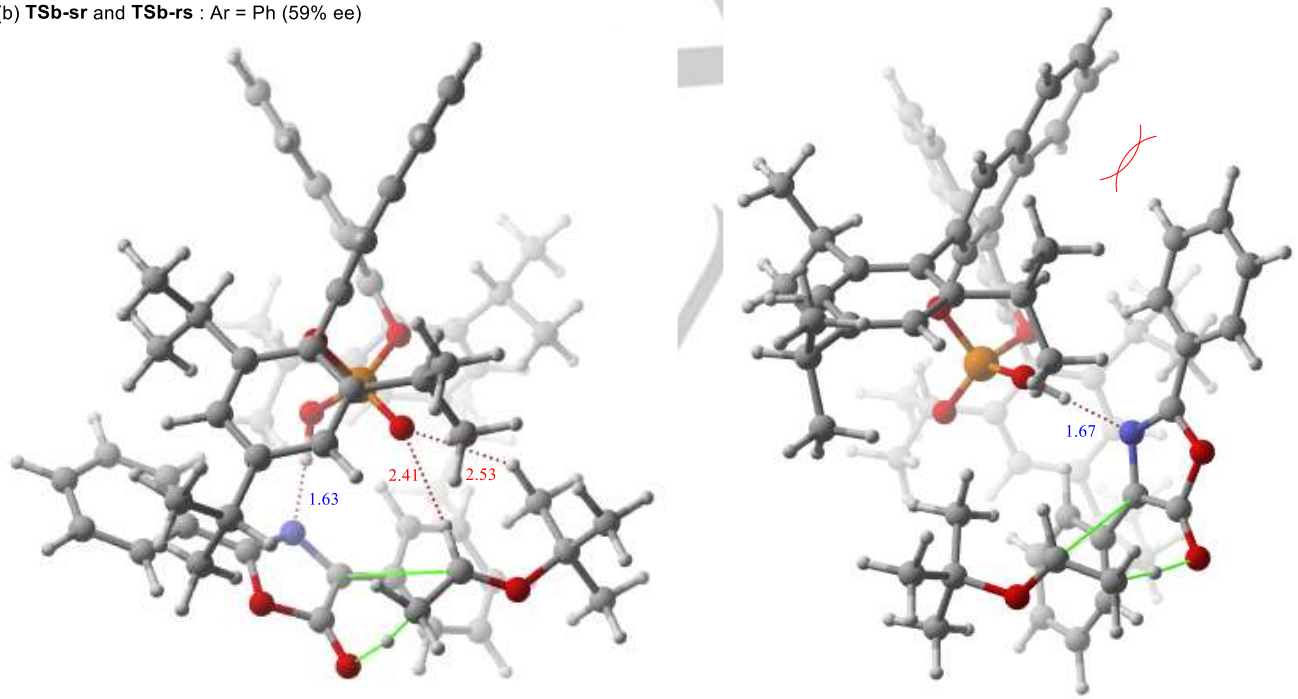

TSb-sr
(0.0 kcal/mol)

TSb-rs
(+1.9 kcal/mol)

Figure 6. 3D structures of (a) **TSa-sr** and **TSa-rs**, which result in *syn*-**5a** (Ar = 3,5-$(MeO)_2C_6H_3$-), and (b) **TSb-sr** and **TSb-rs**, which result in *syn*-**5b** (Ar = Ph). Steric repulsions are indicated by red curves. Hydrogen bonds are represented by red dashed lines. N···H and O···H distances are indicated in blue and red, respectively (angstroms). Bond formation/dissociation is indicated by green solid lines.

10.1002/chem.201905296

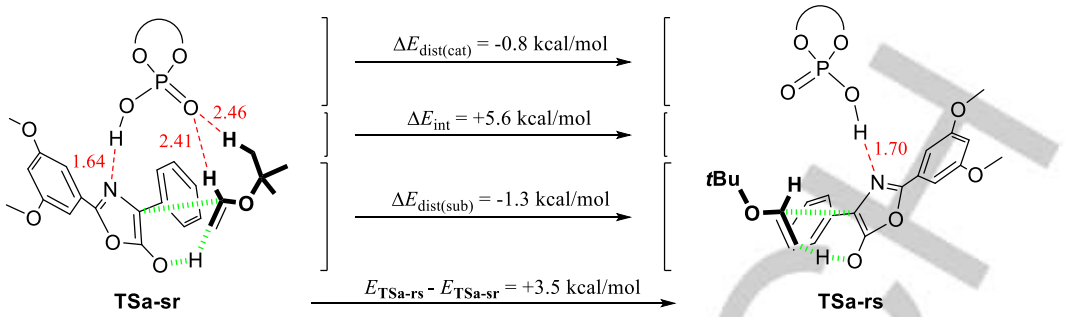

Figure 7. Distortion/interaction analysis for **TSa-sr** and **TSa-rs**. Hydrogen bonds are represented by red dashed lines, and bond formation/dissociation is indicated by green dashed lines. Bond lengths are indicated in red (angstroms).

of the azlactone substituent (Ar) plays a vital role in determining the stereochemical outcome.

As the steric repulsion between azlactone **3** and the backbone of catalyst **1** is the dominant factor influencing the enantioselection, replacement of the Ar group of the azlactone with another bulky group should maintain the relative energy difference between the transition states. Indeed, the calculation for the reaction of azlactone **3c** (Ar = 3,5-$Me_2C_6H_3$-) predicted a sufficient relative energy difference between corresponding **TSc-sr** and **TSc-rs** (3.3 kcal/mol, Figure S7a), although the value was slightly lower than that for the reaction of **3a** (3.5 kcal/mol, Figures 5 and 6a). On the other hand, replacement of **3a** in the transition structures with sterically less hindered **3d** (Ar = 4-ClC_6H_4-) considerably reduced the relative energy difference between corresponding **TSd-sr** and **TSd-rs**, as expected (1.7 kcal/mol, Figure S7b). As mentioned above, the marked substituent effect was pointed out by the theoretical studies. The present effect stems from that the binaphthyl backbone of the catalyst locates in close proximity, particularly in less favorable **TSx-rs**s (**TSx** = **TSa**–**TSd**), to the Ar substituent introduced at the 2-position of azlactone, because the catalyst protonates the nitrogen atom next to the carbon atom substituted by the Ar substituent. Otherwise, the present substituent effect would not be expected.

Table 1. Enantioselective Direct Aldol-Type Reaction of Vinyl Ether **2a** with Azlactones **3** Catalyzed by (*R*)-**1**.[a]

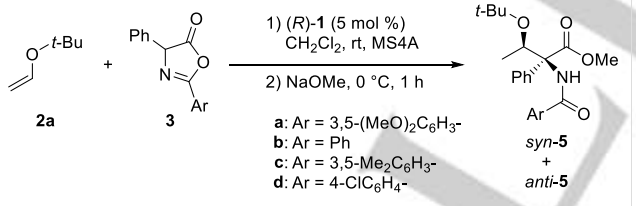

2a **3**

entry	**3**	**5**	Time [h]	Yield [%][b]	*syn*:*anti*[c]	ee [%][c,d] for *syn*-**5**
1	**3a**	**5a**	4	85	95:5	95 (3.5)
2	**3b**	**5b**	24	69	79:21	59 (1.9)
3	**3c**	**5c**	24	60	81:19	73 (3.3)
4	**3d**	**5d**	24	79	75:25	46 (1.7)

[a] All reactions were performed using 0.01 mmol of (*R*)-**1** (5 mol %), 0.4 mmol of **2a** (2.0 equiv), 0.2 mmol of **3**, and 100 mg of MS4A in 0.4 mL of CH_2Cl_2 at room temperature. [b] Combined yield of *syn*/*anti*-**5**. [c] Determined by chiral stationary phase HPLC analysis. [d] The relative energy differences of the transition states, ΔE = $E_{TSx\text{-}rs}$ - $E_{TSx\text{-}sr}$ (kcal/mol) (**TSx** = **TSa**–**TSd**), are shown in parentheses.

Experimental Support

In order to confirm the model for stereocontrol as proposed above, the reactions of **2a** with **3a**–**3d** were performed using (*R*)-**1** as the catalyst under the same conditions (room temperature in dichloromethane).[7a,24] The reaction proceeded in moderate to good yields in a *syn*-selective fashion (Table 1). As expected, the reaction using **3c** afforded corresponding product **5c** with relatively high enantiomeric excess (Table 1, entry 3). On the other hand, the use of **3d** dramatically decreased the enantioselectivity (Table 1, entry 4). The experimentally observed results were in good agreement with the computationally predicted stereochemical outcomes, thus confirming the above proposed model for stereocontrol in the phosphoric acid-catalysed reaction of azlactones with vinyl ethers.

Conclusions

The mechanism for the enantioselective aldol-type reaction of vinyl ethers with azlactones catalysed by chiral phosphoric acid was investigated. DFT studies using a simplified chemical model revealed that the reaction proceeds *via* a six-membered cyclic transition state. In the favorable transition state, phosphoric acid (P-O<u>H</u>) protonates the nitrogen atom of azlactone, whereas the phosphoryl oxygen (P=<u>O</u>) of the catalyst interacts with the vinyl proton of vinyl ether. It is noteworthy that these hydrogen bonds are not involved in the bond recombination sequence and the catalyst functions as a template for binding both substrates, azlactone and vinyl ether, of which relative locations are fixed. Therefore, the present template effect is beneficial not only for stabilizing the transition structures but also for controlling the stereochemical outcome. Further analysis of the realistic chemical model, coupled with experimental support, clarified that the steric repulsion between

the substituent (Ar) of the azlactone and the binaphthyl backbone of the catalyst is also crucial for the enantioselection. The present finding, namely, the template effect, is regarded as one of the key stereocontrolling systems in chiral phosphoric acid catalysis and hence, expands the scope of enantioselective reactions catalysed by chiral phosphoric acids and their derivatives. Further studies on the development of enantioselective reactions using the present intriguing effect are in due course in our laboratory.

Acknowledgements

This work was partially supported by a Grant-in-Aid for Scientific Research on Innovative Areas "Advanced Molecular Transformations by Organocatalysts" from MEXT, Japan (No. 23105002 & 23105005) and a Grant in Aid for Scientific Research on Innovative Areas "Hybrid Catalysis for Enabling Molecular Synthesis on Demand" from MEXT, Japan (No. JP17H06447 & JP18H04660). We also thank the Japan Society for the Promotion of Sciences for the JSPS Research Fellowship for Young Scientists (K. K.).

Keywords: Asymmetric Synthesis • Enantioselectivity • DFT • Organocatalysis • Reaction Mechanism

[1] For selected reviews on chiral phosphoric acid catalysts, see; a) T. Akiyama, *Chem. Rev.* **2007**, *107*, 5744-5758; b) M. Terada, *Synthesis* **2010**, 1929-1982; c) D. Kampen, C. M. Reisinger, B. List, *Top. Curr. Chem.* **2010**, *291*, 395-456; d) D. Parmar, E. Sugiono, S. Raja, M. Rueping, *Chem. Rev.* **2014**, *114*, 9047-9153.

[2] For comprehensive reviews on organocatalysts, see; a) *Science of Synthesis*, *Asymmetric Organocatalysis 1*, *Lewis Base and Acid Catalysts* (Ed.: B. List), Georg Thieme Verlag KG, New York, **2012**; (b) *Science of Synthesis*, *Asymmetric Organocatalysis 2*, *Brønsted Base and Acid Catalysts*, *and Additional Topics* (Ed.: K. Maruoka), Georg Thieme Verlag KG, New York, **2012**.

[3] For seminal works of chiral phosphoric acid catalysts, see; a) T. Akiyama, J. Itoh, K. Yokota, K. Fuchibe, *Angew. Chem., Int. Ed.* **2004**, *43*, 1566-1568; b) D. Uraguchi, M. Terada, *J. Am. Chem. Soc.* **2004**, *126*, 5356-5357. For catalytically active species, also see; c) M. Hatano, K. Moriyama, T. Maki, K. Ishihara, *Angew. Chem. Int. Ed.* **2010**, *49*, 3823-3826; d) M. Terada, K. Kanomata, *Synlett* **2011**, 1255-1258.

[4] For a review of computational studies of organocatalytic reactions, see P. H.-Y. Cheong, C. Y. Legault, J. M. Um, N. Çelebi-Ölçüm, K. N. Houk, *Chem. Rev.* **2011**, *111*, 5042-5137.

[5] For a review of computational studies of chiral Brønsted acid catalysis, see R. Maji, S. C. Mallojjala, S. E. Wheeler, *Chem. Soc. Rev.* **2018**, *47*, 1142-1158.

[6] For representative and recent examples of computational studies of chiral Brønsted acid catalysis, see; a) L. Simón, J. M. Goodman, *J. Am. Chem. Soc.* **2008**, *130*, 8741-8747; b) M. Yamanaka, T. Hirata, *J. Org. Chem.* **2009**. *74*, 3266-3271; c) K. Mori, Y. Ichikawa, M. Kobayashi, Y. Shibata, M. Yamanaka, T. Akiyama, *J. Am. Chem. Soc.* **2013**, *135*, 3964-3970; d) M. N. Grayson, J. M. Goodman, *J. Am. Chem. Soc.* **2013**, *135*, 6142-6148; e) Y. Shibata, M. Yamanaka, *J. Org. Chem.* **2013**, *78*, 3731-3736; f) I. Čorić, J. H. Kim, T. Vlaar, M. Patil, W. Thiel, B. List, *Angew. Chem. Int. Ed.* **2013**, *52*, 3490-3493; g) K. Kanomata, Y. Toda, Y. Shibata, M. Yamanaka, S. Tuzuki, I. D. Gridnev, M. Terada, *Chem. Sci.* **2014**, *5*, 3515-3523; h) M. Terada, T. Komuro, Y. Toda, T. Korenaga, *J. Am. Chem. Soc.* **2014**, *136*, 7044-7057; i) Y. Y. Khomutnyk, A. J. Argüelles, G. A. Winschel, Z. Sun, P. M. Zimmerman, P. Nagorny, *J. Am. Chem. Soc.* **2016**, *138*, 444-456; j) K. Kanomata, M. Terada, *Synlett* **2016**, *27*, 581-585; k) F. Li, T. Korenaga, T. Nakanishi, J. Kikuchi, M. Terada, *J. Am. Chem. Soc.* **2018**, *140*, 2629-2642; l) J. Zhang, P. Yu, S.-Y. Li, H. Sun, S.-H. Xiang, J. Wang, K. N. Houk, B. Tan, *Science* **2018**, *361*, 8707-8710; m) M. Shimizu, J. Kikuchi, A. Kondoh, M. Terada, *Chem. Sci.* **2018**, *9*, 5747-5757; n) J. Kikuchi, H. Aramaki, H. Okamoto, M. Terada, *Chem. Sci.* **2019**, *10*, 1426-1433; o) Y. Kwon, J. Li, J. P. Reid, J. M. Crawford, R. Jacob, M. S. Sigman, F. D. Toste, S. J. Miller, *J. Am. Chem. Soc.* **2019**, *141*, 6698-6705.

[7] a) M. Terada, H. Tanaka, K. Sorimachi, *J. Am. Chem. Soc.* **2009**, *131*, 3430-3431; b) J. Jiang, J. Qing, L.-Z. Gong, *Chem.-Eur. J.* **2009**, *15*, 7031-7034; c) M. Terada, K. Moriya, K. Kanomata, K. Sorimachi, *Angew. Chem. Int. Ed.* **2011**, *50*, 12586-12590; d) E. P. Ávila, R. M. S. Justo, V. P. Goncalves, A. A. Pereira, R. Diniz, G. W. Amarante, *J. Org. Chem.* **2015**, *80*, 590-594; e) C. Ma, J.-Y. Zhou, Y.-Z. Zhang, G.-J. Mei, F. Shi, *Angew. Chem. Int. Ed.* **2018**, *57*, 5398-5402; f) M. Zhang, C. Yu, J. Xie, X. Xun, W. Sun, L. Hong, R. Wang, *Angew. Chem. Int. Ed.* **2018**, *57*, 4921-4925; g) J. Kikuchi, M. Terada, *Angew. Chem. Int. Ed.* **2019**, *58*, 8458-8462.

[8] For reviews of azlactones in organic synthesis, see; a) J. S. Fisk, R. A. Mosey, J. J. Tepe, *Chem. Soc. Rev.* **2007**, *36*, 1432-1440; b) N. M. Hewlett, C. D. Hupp, J. J. Tepe, *Synthesis* **2009**, 2825-2839; c) A.-N. R. Alba, R. Rios, *Chem.-Asian J.*, **2011**, *6*, 720-734; d) P. P. de Castro, A. G. Carpanez, G. W. Amarante, *Chem. Eur. J.* **2016**, *22*, 10294-10318; e) I. F. S. Marra, P. P. de Castro, G. W. Amarante, *Eur. J. Org. Chem.* **2019**, 5830-5855.

[9] For 3,5-dimethoxyphenyl substituted azlactones as an efficient substrate for enantioselective transformations, see; G. Lu, V. B. Birman, *Org. Lett.* **2011**, *13*, 356-358.

[10] a) J. S. Fisk, J. J. Tepe, *J. Am. Chem. Soc.* **2007**, *129*, 3058-3059; b) R. A. Mosey, J. S. Fisk, T. L. Friebe, J. J. Tepe, *Org. Lett.* **2008**, *10*, 825-828.

[11] M. J. Frisch, et al. *Gaussian 09, Revision C.01*, Gaussian, Inc., Wallingford CT, **2010**. See SI for the full list of the authors.

[12] a) A. D. Becke, *Phys. Rev. A*, **1988**, *38*, 3098-3100; b) C. Lee, W. T. Yang, R. G. Parr, *Phys. Rev. B* **1988**, *37*, 785-789.

[13] For M06-2X, see: Y. Zhao, D. G. Truhlar, *Theor. Chem. Acc.* **2008**, *120*, 215-241.

[14] See SI for less stable other tansition structures (Figures S1 and S2).

[15] No transition structure of Path B could be located in the solution phase even by thorough screening for initial structures and optimization methods. However, during the course of this investigation, other transition state **TS-B'** was identified in the solution phase, which affords an acetal product in the reaction of vinyl ether with phosphoric acid (Figure S2). The relative energy for **TS-B'** (ΔE = 8.9 kcal/mol [ΔG = 28.9 kcal/mol]) is higher than that for **TS-C** (ΔE = 3.5 kcal/mol [ΔG = 25.6 kcal/mol]) but lower than that for **TS-A** (ΔE = 16.9 kcal/mol [ΔG = 45.0 kcal/mol]). Although the transition structure of the acetal formation reaction, instead of Path B, was identified in the solution phase, Path C is the most favorable among the pathways investigated.

[16] Single-point energy calculations of the optimized transition states were conducted at the same level in the solution phase according to the SCRF method based on CPCM (CH_2Cl_2). As the result, relative energies of the transition state were calculated to be: Path A: +18.4 kcal/mol, Path B: +12.1 kcal/mol, Path C: +8.2 kcal/mol. See SI for details (Figure S1).

[17] The effective electron delocalization through attractive non-covalent interaction between **AZ** and **VE** in **TS-C** was confirmed by NCIPLOT. See SI for details (Figure S3).

[18] See SI for ^{1}H NMR monitoring in details (Figures S8-S11).

[19] The relative stereochemistry of the product was determined by X-ray crystrallographic analysis, and the absolute stereochemistry at the C3

10.1002/chem.201905296

position of the product was determined by modified Mosher's method. See Ref. 7a for details.

[20] See SI for the structures of **TSa-rr** and **TSa-ss**, both of which afford enantiomers of the *anti*-isomer (Figure S4).

[21] The geometrical optimization of transition states **TSa-sr** and **TSa-rs** was also conducted at the B3LYP-D/6-31G* level. Single-point energy calculations of the optimized structures were performed at the same level with the SCRF method based on CPCM (CH_2Cl_2). Relative energy difference in the solution phase was calculated to be 3.2 kcal/mol in favor of **TSa-sr** (Figure S5). Similarly, identification of transition states **TSa-sr** and **TSa-rs** using the M06-2X/6-31G* level, followed by single-point energy calculations of the optimized structures at the same level with the SCRF method based on CPCM (CH_2Cl_2), was also conducted. Relative energy difference in the solution phase was calculated to be 2.4 kcal/mol in favor of **TSa-sr** (Figure S5).

[22] 3D representations were prepared using CYLview. C. Y. Legault, CYLview, 1.0b; Université de Sherbrooke, **2009** (http://www.cylview.org).

[23] The distortion/interaction analysis was performed by means of the counterpoise method. The computational details are shown in SI. For the original distortion/interaction analysis, see: a) K. Morokuma, K. Kitaura in *Chemical Applications of Atomic and Molecular Electrostatic Potentials* (Eds.: P. Politzer, D. G. Truhlar), Plenum, New York, **1981**. For selected examples using the distortion/interaction analysis, see: b) D. N. Ess, K. N. Houk, *J. Am. Chem. Soc.* **2007**, *129*, 10646-10647; c) D. H. Ess, K. N. Houk, *J. Am. Chem. Soc.* **2008**, *130*, 10187-10198; d) Y.-H. Lam, P. H.-Y. Cheong, J. M. Blasco Mata, S. J. Stanway, V. R. Gouverneur, K. N. Houk, *J. Am. Chem. Soc.* **2009**, *131*, 1947-1957; e) R. S. Paton, S. Kim, A. G. Ross, S. J. Danishefsky, K. N. Houk, *Angew. Chem., Int. Ed.* **2011**, *50*, 10366-10368. f) A. G. Green, P. Liu, C. A. Merlic, K. N. Houk, *J. Am. Chem. Soc.* **2014**, *136*, 4575-4583; g) M. Odagi, K. Furukori, Y. Yamamoto, M. Sato, K. Iida, M. Yamanaka, K. Nagasawa, *J. Am. Chem. Soc.* **2015**, *137*, 1909-1915.

[24] Molecular sieves 4A was added to improve the reproducibility of the reaction outcomes.

10.1002/chem.201905296

WILEY-VCH

FULL PAPER

Entry for the Table of Contents (Please choose one layout)

Layout 1:

FULL PAPER

The mechanism of chiral phosphoric acid-catalyzed aldol-type reaction of azlactones with vinyl ethers was investigated. A Conia-ene-type transition state consisting of the vinyl ether and the enol tautomer of the azlactone was identified on the basis of DFT calculations. Although hydrogen bonds are formed between the catalyst and the substrates, these are not involved in the bond recombination sequence and hence the catalyst functions as a template for binding the substrates.

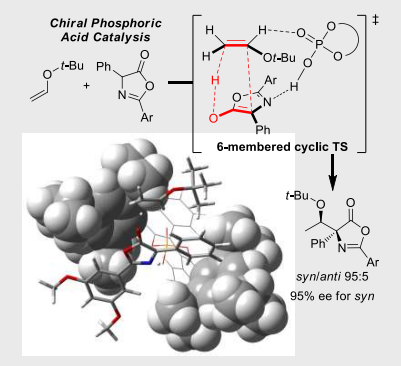

Dr. Kyohei Kanomata, Yuki Nagasawa, Yukihiro Shibata, Prof. Dr. Masahiro Yamanaka, Fuyuki Egawa, Dr. Jun Kikuchi, and Prof. Dr. Masahiro Terada**

Page No. – Page No.

Mechanism and Origin of Stereoselectivity in Chiral Phosphoric Acid-Catalysed Aldol-Type Reactions of Azlactones with Vinyl Ethers

Layout 2:

FULL PAPER

((Insert TOC Graphic here; max. width: 11.5 cm; max. height: 2.5 cm))

*Author(s), Corresponding Author(s)**

Page No. – Page No.

Title